



NIH Public Access

Author Manuscript

Biochim Biophys Acta. Author manuscript; available in PMC 2013 February 1.

Published in final edited form as:

Biochim Biophys Acta. 2012 February ; 1818(2): 263–271. doi:10.1016/j.bbamem.2011.09.011.

A Gate-Free Pathway for Substrate Release from the Inward-Facing State of the Na⁺-Galactose Transporter

Jing Li and Emad Tajkhorshid*

Department of Biochemistry, College of Medicine, Beckman Institute, and Center for Biophysics and Computational Biology, University of Illinois at Urbana-Champaign, Urbana, Illinois 61801, U.S.A

Abstract

Employing molecular dynamics (MD) simulations, the pathway and mechanism of substrate unbinding from the inward-facing state of the Na⁺-coupled galactose transporter, vSGLT, have been investigated. During a 200-ns equilibrium simulation, repeated spontaneous unbinding events of the substrate from its binding site have been observed. In contrast to the previously proposed gating role of a tyrosine residue (Y263), the unbinding mechanism captured in the present equilibrium simulation does not rely on the displacement and/or rotation of this side chain. Rather, the unbinding involves an initial lateral displacement of the substrate out of the binding site which allows the substrate to completely emerge from the region covered by the side chain of Y263 without any noticeable conformational changes of the latter. Starting with the snapshots taken from this equilibrium simulation with the substrate outside the binding site, steered MD (SMD) simulations were then used to probe the translocation of the substrate along the remaining of the release pathway within the protein's lumen and to characterize the nature of protein-substrate interactions involved in the process. Combining the results of the equilibrium and SMD simulations, we provide a description of the full translocation pathway for the substrate release from the binding site into the cytoplasm. Residues E68, N142, T431, and N267 facilitate the initial substrate's displacement out of the binding site, while the translocation of the substrate along the remainder of the exit pathway formed between TM6 and TM8 is facilitated by H-bond interactions between the substrate and a series of conserved, polar residues (Y138, N267, R273, S365, S368, N371, S372, and T375). The observed molecular events indicate that no gating is required for the release of the substrate from the crystallographically captured structure of the inward-facing state of SGLT, suggesting that this conformation might represent an open, rather than occluded, state of the transporter.

Introduction

As a major class of membrane transporters, secondary transporters use the energy stored in transmembrane electrochemical gradient of one solute to power uphill translocation of another (1–5). A large number of secondary transporters use the electrochemical gradients of various ions across the membrane, most prominently Na⁺ or H⁺ ions for their function, and are, therefore, termed ion-coupled secondary transporters. Accumulating evidence from biochemical, kinetic, and structural studies have established that, similar to other

© 2011 Elsevier B.V. All rights reserved.

*Corresponding author: emad@life.illinois.edu; phone: +1-217-244-6914.

Publisher's Disclaimer: This is a PDF file of an unedited manuscript that has been accepted for publication. As a service to our customers we are providing this early version of the manuscript. The manuscript will undergo copyediting, typesetting, and review of the resulting proof before it is published in its final citable form. Please note that during the production process errors may be discovered which could affect the content, and all legal disclaimers that apply to the journal pertain.

transporters, all ion-coupled transporters operate via the so-called alternating-access mechanism, in which during the transport cycle the transporter protein undergoes conformational transitions between two major states, an inward-facing (IF) and an outward-facing (OF) one, thereby switching the substrate access between the two sides of the membrane (6, 7).

Recent years have seen an increasing number of high-resolution crystal structures of secondary transporters. Surprisingly, despite broad diversity in the transported substrate and ions, a large number of secondary transporters, including both antiporters and symporters, bear significant architectural resemblance – two structural inverted repeats, each with a set of five transmembrane helices (TMs) oppositely oriented with respect to the membrane. These include leucine transporter (LeuT) (8–10), bacterial Na⁺-coupled galactose transporter (vSGLT) (11, 12), the benzyl-hydantoin transporter (Mhp1) (13, 14), betaine transporter (BetP) (15), carnitine transporter (CaiT) (16, 17), Na⁺-independent amino acid transporter (ApcT) (18), and arginine:agmatine antiporters (AdiC) (19–22). The common architecture among these transporters has been termed the LeuT-fold architecture, due to the fact LeuT was the first among the group to be structurally characterized at high resolution (23).

Structural alignment of these transporters indicates a close similarity in the location of the substrate binding sites of LeuT, Mhp1, vSGLT and BetP, which in all cases, is formed at the interface of the two inverted structural repeats (23, 24). Sequence and structural comparisons of LeuT, Mhp1, vSGLT, and ApcT also suggest a conserved cation binding site which is named as the Na2 binding site in LeuT and found to be critical for substrate binding and symport in various LeuT-fold transporters (18, 23–25). These structural similarities suggest that the secondary transporters of the LeuT-fold topology might present a growing superfamily that share a similar mechanism of transport.

Despite the fast progress over the last few years in structural biology of membrane proteins, structural information on membrane transporters is still scarce, and for most of them no structures are yet available. In the majority of structurally characterized transporters, only one state could be experimentally captured. The functional state represented by the structurally determined state is, however, not always easy to characterize. Specifically, it is sometimes difficult to judge whether the structure represents an open, closed, or semi-occluded state on the two ends (cytoplasmic and periplasmic/extracellular) of the transporter protein. In other words, it is not clear whether the substrate and/or the co-transported ions as well as water molecules have full, partial, or no access to their respective binding sites within the protein lumen. Furthermore, although by combining the available crystal structures of different proteins in the LeuT-fold family we have achieved a uniquely well resolved description of the number of states involved in the transport cycle of this family, the nature of the structural transitions involved, and how they underlie the transport mechanism, are still far from well understood. Another important mechanistic aspect regards the sequence of binding and unbinding events for the substrate and the co-transported ion(s) during the cytoplasmic and extracellular transport half-cycle, which is poorly understood for the majority of secondary membrane transporters. Describing such mechanistic details based on static structures is rather challenging and calls for methodologies that can offer a dynamical treatment of the protein of interest.

As the first IF structural state of a LeuT-fold transporter, the structure of vSGLT (11) provided crucial information toward better characterization of the alternating-access mechanism and the sequence of molecular events in these transporters. Although the sequence of binding events from the extracellular side has been partially characterized for vSGLT and hSGLT1 (the homologous human Na⁺/glucose transporter) experimentally (26–28), the sequence and the mechanism of unbinding of the transported species from the

protein into the cytoplasmic side are largely unknown. While the presence of the co-transported Na^+ ion in the protein could not be unequivocally determined using the experimental data, in the reported PDB file, a Na^+ ion was modeled in a putative binding site corresponding to that of the homologous protein LeuT based on the structural alignment and mutagenesis results (11).

This functionally relevant feature turned out to be the first to be studied using molecular dynamics (MD) simulations (12, 29, 30). In the first report, repeated equilibrium MD simulations together with detailed structural comparison of the Na^+ -binding sites of vSGLT and LeuT were used to argue against the presence of an ion in the protein, proposing that the crystallographically captured structure represents an ion-free state (29). These results were consistently reproduced by simulations from other laboratories (12, 30) establishing the notion that the crystal structure is the state in which the ion binding site has sufficiently opened to allow the release of the Na^+ ion (24, 31), while the substrate is still bound to the transporter.

The next step along the transport cycle is the release of the substrate from its own binding site into the cytoplasmic solution. Based on the crystal structure, it is not easy to determine to what degree the substrate binding site is accessible from outside solution, especially after taking into account the effect of thermal fluctuation of the protein. In other words, it is not clear whether further protein conformational changes are required, and if so to what degree, for the release of the substrate into the cytoplasmic solution. In membrane transporters, the transition between major functional states is coupled to either global protein conformational changes, which usually involve several TM helices, e.g., transition between the IF and OF states of Mhp1 (14), or more localized gating motions of a few residues e.g., the inward bending of the N-terminal half of TM10 in Mhp1 observed after substrate binding (13).

In the crystal structure (11), the substrate is bound about halfway across the membrane with its binding site flanked by hydrophobic residues on both the cytoplasmic and extracellular sides. On the cytoplasmic side, Y263 from the broken helix TM6E stacks with the pyranose ring of the galactose (Fig. 1), a feature commonly found in a sugar-binding proteins (32, 33). The position of this residue along a pathway that linearly connects the substrate to the cytoplasmic opening of the lumen triggered the idea that Y263, together with the flanking residues Y262 and W264, might play the role of the cytoplasmic gate, and that the crystal structure represents a substrate-occluded state in which the exit of the substrate toward the cytoplasmic solution is blocked by Y263 (11). Based on this mechanism, the release of the substrate from its binding site would rely on either large conformational changes of the TM region of the protein, or more likely, a gate-like, side-chain motion of Y263 and/or its neighboring residues that would further open the cytoplasmic lumen and increase the substrate accessibility. Two independent simulation studies in which the translocation of the substrate from its binding site toward the cytoplasmic solution was induced by either umbrella sampling or steered molecular dynamics (SMD) have presented results supporting the notion that Y263 plays a gating role in the cytoplasmic lumen of vSGLT. In both simulations, the translocation of the substrate toward the cytoplasmic solution required/was accompanied by side-chain rotation of Y263 (12, 30).

Here, we report the results of an extended equilibrium MD simulation of a membrane-embedded model of vSGLT (200 ns), in which a distinct pathway and a novel mechanism for substrate release from the state captured in the crystal structure are presented. In contrast to previously reported mechanisms, our simulation describe a substrate unbinding pathway in which the substrate takes a curved pathway around the seemingly gate-like side chain of Y263. The substrate complete release from its original binding site is captured in full in this equilibrium simulation without the need of any conformational changes to the surrounding

residues, in particular that of Y263. We argue that our mechanism involving a gate-free pathway for substrate release from vSGLT is in a much closer agreement with the recent crystal structure of substrate-free vSGLT (12), in which the position of the “gating” side chain is essentially identical to that of the substrate-bound form (11).

Materials and Methods

Model building

The simulation system was constructed by embedding monomeric vSGLT including the bound substrate galactose, which was taken from the RCSB Protein Data Bank (PDB ID: 3DH4) (11) into a lipid bilayer, as described in detail below. The titration states of ionizable residues (aspartate, glutamate, lysine, arginine, histidine, and tyrosine) were assigned based on pK_a calculations performed using the H++ server (34), which resulted in a model in which all residues have their default titration states. Coordinates for the six missing residues (179–184) were constructed using the Psfgen plugin of VMD (35) employing the CHARMM27 topology file for proteins (36–38). The first 46 N-terminal residues, including unassigned residues (3–19) of helix –1 (helix numbering based on the recent convention used for inverted repeat symporters (23)) and the unresolved loop (residues 20–46) were not included in the model. These residues do not belong to the core structure of the transporter, and thus are not expected to be essential for the mechanism.

About 150 water molecules were added using DOWSER (39) to the protein. The first principal axis of the protein was aligned with the z axis using the OPM (Orientations of Proteins in Membranes) database (40). Then, the system was inserted into a patch of POPE (1-palmitoyl-2-oleoyl-*sn*-glycero-3-phosphatidylethanolamine) bilayer ($100 \times 100 \text{ \AA}^2$) generated using the Membrane Builder plugin of VMD (35) with the membrane normal along the z -axis. The lipid molecules overlapping with the protein were deleted. The system was then solvated using the program SOLVATE (41), and water molecules in the lipid-protein interface were deleted. The simulation system was then neutralized with 100 mM NaCl using the Autoionize plugins of VMD (35). The final dimensions of the system before equilibration were $100 \times 98 \times 95 \text{ \AA}^3$ including ~85,000 atoms.

Simulation protocol

All the simulations were performed using NAMD 2.6 (42), the CHARMM27 force field (37) for proteins, lipids, ions and the substrate galactose (43), and TIP3P model for explicit water (44). All the simulations were performed under periodic boundary conditions with a time step of 2 fs. Throughout the simulations, bond distances involving hydrogen atoms were fixed using the SHAKE algorithm (45). After an initial 1000 steps of minimization, lipid tails were *melted* in a 500-ps NVT (constant volume and temperature) simulation at 310 K, during which all atoms except the lipid tails were fixed. The system was then equilibrated in an NPT (constant pressure and temperature) ensemble with a constant pressure of 1 atm for 500 ps, during which all heavy atoms of the protein, the substrate and the bound Na^+ ion were constrained by harmonic potentials ($k = 7.2 \text{ kcal/mol}/\text{\AA}^2$) to allow for relaxation and packing of the lipid molecules and water around the protein. After a 500-ps NPT MD with heavy atoms constrained, and a 2.5–ns unconstrained NPT simulation, the production run was performed for 200 ns in an NP_nT ensemble (constant area, temperature, and normal pressure) under equilibrium conditions.

Although two complete substrate unbinding events from its binding site were captured spontaneously during the equilibrium simulation, to probe the remainder of the exit pathway from the protein lumen into the cytoplasmic milieu, and to probe potential barrier regions along the unbinding pathway, four SMD simulations were also performed, each starting

from a different snapshot taken from the equilibrium trajectory (snapshots at 0, 89, 115, and 155 ns) representing typical different configurations of the substrate during the production run. We employed the protocol of constant-velocity (cv) SMD (cv-SMD (46, 47)), with the arising force applied to the substrate's center of mass toward the cytoplasmic side of the protein. The force was directed along the z axis (membrane normal) and was defined positive for pulling toward the cytoplasmic direction (Fig. 1). A force constant of $k = 7$ kcal/mol/Å² and a pulling speed of $v_z = 2$ Å/ns were used for the SMD simulations. The C_α atoms of three remote residues from the translocation pathway (S313, I413, and F472) were fixed to prevent the overall translation of the system in response to the applied external force.

For all the MD and SMD simulations, constant temperature was maintained by employing Langevin dynamics with a damping coefficient of 0.5 ps⁻¹. The Langevin piston method (48, 49) with a piston period of 100 fs was used to maintain the pressure at 1.0 atm. Short-range non-bonded interactions were calculated using a cutoff distance of 12 Å, and long-range electrostatic forces were described using the particle mesh Ewald (PME) method (50).

Results and Discussion

Capturing Spontaneous Substrate Unbinding

In order to investigate the dynamics of the IF state of vSGLT in its substrate-bound form, a 200-ns equilibrium MD simulation was performed on the membrane-bound model of the transporter. During the simulation, vSGLT maintains its IF state with the protein's backbone RMSD invariably below 3 Å throughout the trajectory. We note that the initially bound Na⁺ ion reported in the crystal structure (11) was released rapidly (within a few nanoseconds) from the protein into the cytoplasmic solution during the initial phase of the simulation. This feature has been uniformly observed in all previous simulations of vSGLT reported by our laboratory (29), as well as those reported later by other groups (12, 30). As put forward earlier (29), we associate this observation with the crystal structure of vSGLT representing a Na⁺-free state, a hypothesis which is supported by structural comparison of the ion binding site in vSGLT and in other structurally known LeuT-fold transporters (29), e.g., LeuT (8) and Mhp1 (13). Therefore, in the following discussion, we will refer to the state simulated in this study simply as the substrate-bound state.

In contrast to the protein, the substrate galactose shows significant fluctuations (Fig. 3A) during the simulation, resulting in its occasional complete displacement from the binding site within the lumen of vSGLT, as monitored by the substrate's heavy atom RMSD and the z -coordinate of its center of mass (Fig. 2A). Note that despite complete unbinding from its binding site, the substrate does not leave the protein lumen during the simulation, and after its apparently barrier-free, back and forth motion outside the binding site, it returns to the binding site region. Nevertheless, the unbinding events from the binding site observed during the simulation clearly capture an initially curved (non-linear) exit pathway for the substrate. Of high relevance to the mechanism of transport in vSGLT is the fact that during the observed unbinding events only marginal conformational changes, even at the level of side chains, were observed to accompany the complete departure of the substrate from its binding site. This is particularly important with regard to Y263, which has been suggested to act as a cytoplasmic gate in vSGLT (12, 30). Based on the equilibrium unbinding events observed in our simulation, we propose that no gating motion is required for the release of the substrate from its binding site in the IF state of vSGLT as captured in the crystal structure (11).

To better characterize the unbinding process, the dynamics of the substrate and its unbinding pathway during the two major unbinding events observed in the simulation are described

here in more detail. The first unbinding event (Unbinding Event I) was captured at $t = 81$ ns, at which point galactose adopts a position that is ~ 7 Å away from its original position towards the cytoplasmic side of the membrane, almost reaching the level of the plane of the aromatic ring of Y263 along the membrane normal ($z = \sim 4$ Å; Fig. 2A). The substrate remains in this position for about 15 ns (Fig. 2A).

Energetic analysis of the trajectory (Table S1) suggests that in the configuration achieved through Unbinding Event I, the substrate has the highest probability to exit the protein, since it experiences the lowest protein-substrate interaction energy and the highest water-substrate interaction energy. During Unbinding Event I (Fig. 3C) the substrate completely moves out of the original binding site, losing almost all of its original contacts with the binding site residues (Q69, E88, S91, N260, and K294), and instead establishes new contacts with several polar residues outside the binding site (N142, N267, T431), as indicated by the calculated contact frequency map (Fig. 2B). During the substrate's exit from the binding site, H-bonds with E68, T431, N142, and N267 appear to facilitate substrate unbinding. Most importantly, the substrate is no longer blocked along its path toward the cytoplasmic solution by Y263, which has been viewed as a "cytoplasmic plug" (Fig. 3C). Supporting the notion of the involvement of these residues in the exit pathway, previous studies have shown that the mutation of the residue corresponding to N142 in the homologous protein SGLT1 (K157A) impairs transport in oocytes (51). The residue corresponding to T431 in vSGLT (T460 in SGLT1) was even suspected to be a substrate-binding residue since its mutation to cysteine altered sugar selectivity and decreased the affinity for glucose (52). Interestingly, neither N142 nor T431 appears to contribute directly to the substrate binding site in the crystal structure (11). The characterized unbinding pathway in our simulation, however, provides a molecular explanation for the importance of these residues and how they might assist the substrate with its unbinding and translocation toward the cytoplasmic side. Examination of the trajectory suggests that, the interaction of the polar side chains of these residues (N142 and T431) with the substrate might be important for facilitating the unbinding of the substrate and its translocation around the major obstacle of Y263. Mutation of either residue to a nonpolar, or even less polar, side chain would therefore be expected to lower the chance of efficient substrate unbinding, as observed experimentally (51, 52).

The displacement of the substrate out of its binding pocket involves a large lateral (parallel to the membrane plane) component, leading to an unbinding mechanism that is independent of the rotation of Y263. In other words, in the pathway captured in our simulation, the substrate goes around the side chain of Y263, an important detail that might be missed if the substrate is pulled linearly toward the cytoplasmic solution. As will be shown later by SMD simulations performed here as well as those reported in a previous simulation study (30), the forced rotation of Y263 appears to be costly and can only be induced by applying rather large forces in the simulations (Table 1). In contrast, the unbinding mechanism captured in our simulation uses a pathway along which the substrate can circumvent the Y263 plug on its exit toward the cytoplasmic milieu.

A second major unbinding event (Unbinding Event II) is captured at $t = 115$ ns, although in this case the substrate diffuses back into the binding site more rapidly (in ~ 1 ns) than in Unbinding Event I. The displacement of the substrate from the binding site in Unbinding Event II is very similar to Unbinding Event I, as the substrate takes the same exact pathway out and reaches approximately the same level ($z = \sim 4$ Å; Fig. 2A) within the protein lumen. The overall displacement of the substrate from its original position in the binding site in Unbinding Event II measures to ~ 7 Å, and during the process it forms contacts with E68, N142, and N267. Similar to Unbinding Event I, the substrate is seen to have completely emerged out of the binding site and uncovered from Y263 along its exit pathway towards the cytoplasmic side (Fig. 3D). We note that the side chain of Y263 in either case does not

undergo any conformational changes during the substrate unbinding (Fig. 5). In both unbinding events, E68 appears to play an important role in facilitating the exit of the substrate from its binding pocket (Table S1). Based on the observed direct interaction with the substrate, we suggest that the mutation of E68 or corresponding residues in other SSS members, especially to an apolar side chain, will have a diminishing impact on the transport efficiency of SGLTs. This remains to be determined experimentally, since to our knowledge, no mutagenesis analysis of the effect of this residue on transport has been reported.

After the significant fluctuations and two complete unbinding events during the first 130 ns of the simulation, the substrate moves back into the binding site and stays there for the rest of the simulation (last 70 ns). The position and the pose of the substrate (Fig. 3E), however, are different from those observed in the crystal structure (Fig. 3B) (11). In this state, which we refer to as the “Silent Phase”, the substrate is closer to the opening of the binding site (Fig. 3E) than in the crystal structure (Fig. 3B) and is stabilized mainly by N64, E68, Q69 and E88 (Fig. 2A). We note that the term “silent” is used to only underline the reduced degree of fluctuation of the substrate during the last phase of the simulation. The transport cycle of SGLTs is approximated to be roughly on the order of tens of milliseconds (53, 54), providing ample time for such transient states, which might not necessarily be needed for the overall transport, to arise and disappear during the full cycle.

The charged side chains of E88 and E68, especially the former, have large contributions to the overall substrate–protein interaction energy in this phase, with E88 responsible for ~ -35 kcal/mol of the total interaction energy of ~ -60 kcal/mol (Table S1). E88 appears to be the main residue forming H–bonds with the substrate, and the number of H–bonds to this side chain shows a strong correlation with the stability of substrate in the trajectory (Fig. S2). Consistent with the major role of E88 in stabilizing the substrate in the binding site as an “anchor”, the mutation of this conserved residue has been shown to abolish Na^+ –dependent galactose transport (11). Breaking from E88 is likely a high-barrier step in the unbinding of the substrate from the transporter. To exemplify the contrast between the bound state and the substrate’s poses achieved during the unbinding events, we note that after Unbinding Event I the E88–substrate interaction energy is dropped to below 1.5 kcal/mol clearly indicating the detachment of the substrate from the binding site.

Water Dynamics and Accessibility of the Substrate Binding Site

The accessibility of binding site to water is a prerequisite for successful substrate unbinding, and the degree of hydration and water dynamics can be viewed as strong measures for the degree of opening of the binding site. While Y263 along with its neighboring residues Y262 and W264 establish a plug-like structure that appears to prevent the linear displacement of the substrate from the binding site toward the cytoplasm, it does not occlude the binding site from water molecules, a finding more consistent with an open state of the binding site. During the simulation, water molecules readily reach the substrate binding site from the cytoplasmic side and form multiple H–bonds with the substrate. Water entrance into the binding site and hydration of the substrate facilitate the unbinding of the substrate by breaking protein–substrate H–bonds. The 80.0–81.5 ns segment of the trajectory provides a good example, during which the approaching water molecules compete with E88 for H–bonding to the substrate and gradually replace the original H–bonds between E88 and the substrate (Fig. S1). Since E88 is responsible for over than half of the protein–substrate interaction energy in the binding site, breaking of its H–bonds to the substrate is critical for freeing the latter from the binding site.

The Unbinding Pathway from the Binding Site to the Cytoplasm

Although the substrate exhibits full unbinding fully from its crystallographically determined binding pocket on several occasions during the equilibrium simulation, it does not completely leave the protein's lumen during the simulated time scale. To explore the remainder of the unbinding pathway for substrate release, two independent SMD simulations were performed starting from the unbound states characterized during the equilibrium simulation, i.e., those obtained after Unbinding Event I and II (snapshots taken at $t = 89$ ns and 115 ns, respectively). In addition, for comparison of the forces required to induce the unbinding, we have also performed two SMD simulations starting from the fully bound state of the substrate, one starting from the initial state which is very close to the crystal structure ($t = 0$ ns), and the other starting from a snapshot representing the Silent Phase of the equilibrium MD simulation ($t = 150$ ns). During the SMD simulations, which are labeled as SMD-I, SMD-II, SMD-III, and SMD-IV, based on the time point of their starting configuration, the force is applied to the center of mass of the substrate along the +z-axis towards the cytoplasmic solution.

A major force peak (~ 1200 pN) is obtained around $t = 2.8$ ns in the force-time profiles of both SMD-I and SMD-IV simulations (both starting from the bound states), which can be clearly attributed to the blocking effect of the aromatic ring of Y263 along the enforced displacement of the substrate linearly toward the cytoplasm (Fig. 4A and D). The substrate passes the physical barrier of Y263 in SMD-I and SMD-IV in two different ways; while in SMD-I, side chain rotation of Y263 allows the substrate to pass, in SMD-IV substrate takes a pathway around Y263 without causing significant rotation of this side chain (Fig. 5). After crossing the apparent barrier of Y263, no comparably large barriers are observed during the remainder of the pulling simulations (Fig. 4A and D). These high-force profiles have also been observed in a previously reported SMD simulation starting from the bound state of the substrate in vSGLT (30). A significantly smoother pathway and lower force profiles are obtained for SMD-II and SMD-III simulations, since in the starting configurations for these simulations the substrate has already completely unbound from its binding site, and is no longer "blocked" by Y263 along the cytoplasmic translocation pathway. No major barriers similar to those observed in SMD-I and SMD-IV are observed for these simulations during the unbinding of the substrate (Fig. 4B and C). While these results agree with the side chain of Y263 introducing a major obstacle along the substrate exit pathway, they also clearly show that the substrate does not have to wait for the conformational change of this residue to overcome the obstacle. During Unbinding Events I or II, the substrate appears to have had time to explore the space available and to have completely circumvented Y263 through lateral displacement, that is perpendicular to the apparent exit pathway. As such, during the subsequent SMD-II and SMD-III simulations, no conformational changes are observed in the rotameric state of Y263 (Fig. 5). The overall structure of the protein remains intact during all of the SMD simulations, and even in SMD-I and SMD-IV simulations where large forces are used to induce likely artificial events, no major conformational changes of the whole protein is observed, suggesting that the conformational state captured in the crystal structure (11) is very close to, if not the same as, the IF open state.

Combining Unbinding Events I and II from the equilibrium simulation and the following smooth exit trajectories of SMD-II and SMD-III, we can describe the complete release pathway for the substrate from the binding site to the cytoplasm (Fig. 6 and Supplementary Movie). We note that the two exit pathways in SMD-II and SMD-III are essentially identical. During the equilibrium unbinding, residues E68, N142, T431, and N267 facilitate the initial lateral translocation of the substrate and its escape from the binding site. Subsequently, the substrate passes through a low-resistance open pathway toward the cytoplasm lined by S365, A63, N267, Y138, S368, S372, Y269, N371, R273, and T375, which are mostly located on TM6 and TM8 helices (Fig. 6). The majority of these polar or

basic residues, most notably an array of equally spaced serine and threonine residues (S365, S368, S372, and T375) from TM8, form direct H–bonds with the substrate, thereby lubricating its passage along the exit pathway (Figs. S3 and S4). Notably, several of these polar residues, namely, Y138, N267, R273, S368, N371, and S372, are highly conserved in Na^+ –coupled sugar symporters of the SSS family, but replaced by nonpolar amino acids in the Proline: Na^+ symporter from the same family (Fig. S5), supporting their importance in facilitating the translocation of sugar substrates. Finally, the characterized substrate exit pathway is through the putative Na^+ binding site (11). In other words, the lumen opening exploited by the substrate to exit the protein coincides with the region that has been proposed to constitute the putative Na^+ binding site. As the substrate directly interacts with the residues of and around this putative Na^+ -binding site, e.g., S365 and A63, it is conceivable that in the presence of a bound Na^+ to this site, the pathway would be at least partially blocked. These observations are in line with our earlier conclusion that cytoplasmic release of Na^+ precedes that of the substrate (29).

Mechanistic Implications

Characterizing the functional state of crystallographically solved structures of membrane transporters is not always straightforward. This is particularly important since significant effort and resources are invested in capturing the protein in different conformational states which might represent functional intermediates involved in the transport cycle. The currently available structures for membrane transporters are generally classified as either inward-facing (IF) or outward-facing (OF) states, and as open or occluded sub–states, primarily based on the degree of accessibility of the substrate binding site from the two sides of the membrane. A major difficulty in this regard is that the degree of accessibility of cavities and openings within the protein mass and lumen cannot be always easily assessed based on static structures. A dynamical description of the structure that accounts for the ability of the lining residues to fluctuate and to form various types and degrees of interaction with incoming molecular species is necessary to know whether a particular conformation is representing a closed/occluded state, a semi-open state, or an open state.

Based on the position and intimate interaction of the substrate and Y263 in its binding site of the substrate-bound structure of IF vSGLT (11), a cytoplasmic gating role for this residue was proposed, and the structure was assigned to represent the IF–occluded state of the transporter. Starting from this structure, simulation studies employing SMD to induce the unbinding of the substrate (30), as well as a more recent study using equilibrium simulations (12) supported the gating role of Y263, since in both studies the exit of the substrate from its binding site was found to depend on the rotation of this residue.

In the equilibrium simulation presented here, we find a completely different mechanism and pathway for cytoplasmic unbinding of the substrate; the substrate main unbinding event is facilitated by its initial lateral displacement parallel to the membrane plane (lateral exit) and through a pathway that takes the substrate around Y263 rather than through it, resulting in an unbinding mechanism that is independent of the rotation of this side chain (Fig. 5). The observed unbinding pathway suggests that in the crystallographically captured structure (11), the substrate already has access to the space outside its binding site, that is, the binding site is in an open state. We note that an open state is in a much closer agreement with the very large fluctuation of the substrate in its binding site, which is consistently observed in all the reported simulations, including the previous two reports that support the gating role of Y263 (12, 30). Furthermore, we argue that the recent crystal structure of IF vSGLT in its substrate–free form (12) is in closer agreement with a gate–free release of the substrate, since in this structure (12), the rotameric state of Y263 is unchanged compared to that in the substrate–bound state (11). Taken together, the high degree of similarity of the binding site

configurations in the two IF structures of vSGLT (11, 12), and the observed spontaneous unbinding of the substrate in the absence of any conformational change in the residues lining the binding site observed in the simulation presented here, lead us to the conclusion that the crystal structure of the substrate-bound vSGLT (11) represents an IF-open state rather than an IF-occluded state. We would like to note that the substrate might still take advantage of the space that might be occasionally and transiently vacated as a result of the rotation of the Y263 side chain, as observed in previous simulations (12, 30), but it does not rely on such a pathway and can take advantage of alternative, more permanently accessible routes for its initial unbinding from the binding pocket.

Supplementary Material

Refer to Web version on PubMed Central for supplementary material.

Acknowledgments

Simulations in this study have been performed using TeraGrid Resources (grant MCA06N060) The study has been supported by National Institutes of Health grants R01-GM086749, R01-GM067887, P41-RR05969, and U54-GM087519.

References

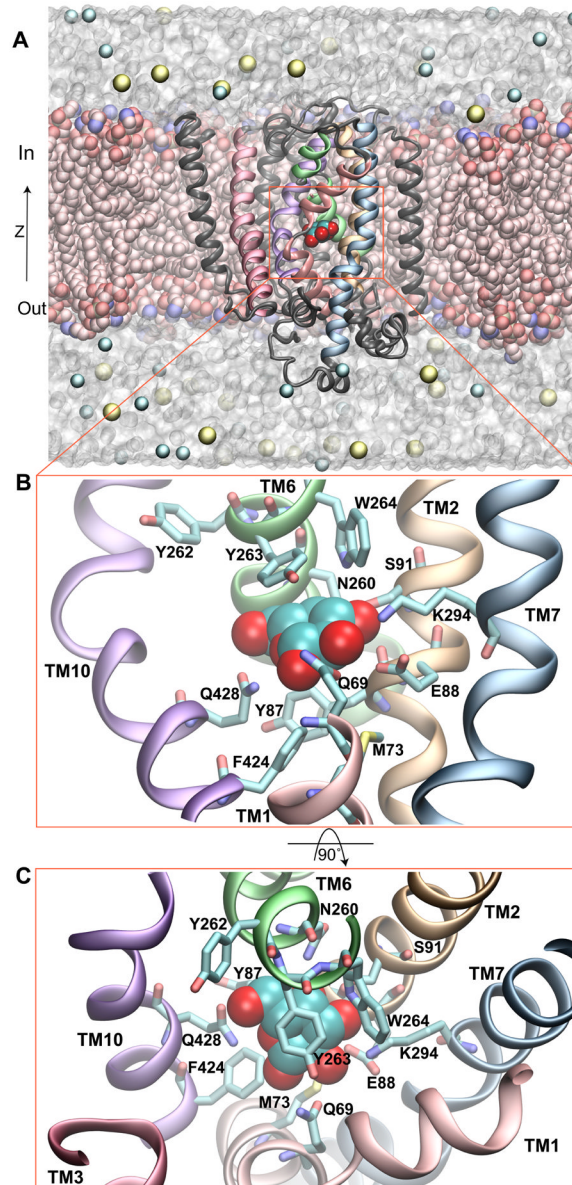
1. Kanner BI. Bioenergetics of neurotransmitter transport. *Biochim Biophys Acta*. 1983; 726:293–316. [PubMed: 6141802]
2. Kanner BI, Schuldiner S. Mechanism of transport and storage of neurotransmitters. *CRC Crit Rev Biochem*. 1987; 22:1–39. [PubMed: 2888595]
3. Kanner BI. Ion-coupled neurotransmitter transport. *Curr Opin Cell Biol*. 1989; 1:735–738. [PubMed: 2576384]
4. Poolman B, Konings W. Secondary solute transport in bacteria. *Biochim Biophys Acta*. 1993; 1183:5–39. [PubMed: 8399376]
5. Forrest LR, Krmer R, Ziegler C. The structural basis of secondary active transport mechanisms. *Biochim Biophys Acta*. 2011; 1807:167–188. [PubMed: 21029721]
6. West IC. Ligand conduction and the gated-pore mechanism of transmembrane transport. *Biochim Biophys Acta*. 1997; 1331:213–234. [PubMed: 9512653]
7. DeFelice LJ. Transporter structure and mechanism. *TRENDS in Neurosciences*. 2004; 27:352–359. [PubMed: 15165740]
8. Yamada S, Pokutta S, Drees F, Weis WI, Nelson WJ. Deconstructing the cadherin-catenin-actin complex. *Cell*. 2005; 123:889–901. [PubMed: 16325582]
9. Zhou Z, Zhen J, Karpowich NK, Goetz RM, Law CJ, Reith MEA, Wang DN. LeuT-Desipramine structure reveals how antidepressants block neurotransmitter reuptake. *Science*. 2007; 317:1390–1393. [PubMed: 17690258]
10. Singh SK, Piscitelli CL, Yamashita A, Gouaux E. A competitive inhibitor traps LeuT in an open-to-out conformation. *Science*. 2008; 322:1655–1661. [PubMed: 19074341]
11. Faham S, Watanabe A, Besserer GM, Cascio D, Specht A, Hirayama BA, Wright EM, Abramson J. The crystal structure of a sodium galactose transporter reveals mechanistic insights into Na⁺/sugar symport. *Science*. 2008; 321:810–814. [PubMed: 18599740]
12. Watanabe A, Choe S, Chaptal V, Rosenberg JM, Wright EM, Grabe M, Abramson J. The mechanism of sodium and substrate release from the binding pocket of vSGLT. *Nature*. 2010; 468:988–991. [PubMed: 21131949]
13. Weyand S, Shimamura T, Yajima S, Suzuki S, Mirza O, Krusong K, Carpenter EP, Rutherford NG, Hadden JM, O'Reilly J, Ma P, Saidijam M, Patching SG, Hope RJ, Norbertczak HT, Roach PCJ, Iwata S, Henderson PJF, Cameron AD. Structure and molecular mechanism of a Nucleobase-Cation-Symport-1 family transporter. *Science*. 2008; 322:709–713. [PubMed: 18927357]

14. Shimamura T, Weyand S, Beckstein O, Rutherford NG, Hadden JM, Sharples D, Sansom MSP, Iwata S, Henderson PJF, Cameron AD. Molecular Basis of Alternating Access Membrane Transport by the Sodium-Hydantoin Transporter Mhp1. *Science*. 2010; 328:470–473.10.1126/science.1186303 [PubMed: 20413494]
15. Ressl S, van Scheltinga ACT, Vonrhein C, Ott V, Ziegler C. Molecular basis of transport and regulation in the Na^+ /betaine symporter BetP. *Nature*. 2009; 458:47–52. [PubMed: 19262666]
16. Tang L, Bai L, Wang WH, Jiang T. Crystal structure of the carnitine transporter and insights into the antiport mechanism. *Nat Struct Mol Biol*. 2010; 17:492–496. [PubMed: 20357772]
17. Schulze S, Koster S, Geldmacher U, van Scheltinga ACT, Kuhlbrandt W. Structural basis of Na^+ -independent and cooperative substrate/product antiport in CaiT. *Nature*. 2010; 467:233–237. [PubMed: 20829798]
18. Shaffer PL, Goehring A, Shankaranarayanan A, Gouaux E. Structure and mechanism of a Na^+ -independent amino acid transporter. *Science*. 2009; 325:1010–1014. [PubMed: 19608859]
19. Fang Y, Jayaram H, Shane T, Kolmakova-Partensky L, Wu F, Williams C, Xiong Y, Miller C. Structure of a prokaryotic virtual proton pump at 3.2 Å resolution. *Nature*. 2009; 460:1040–1043. [PubMed: 19578361]
20. Gao X, Lu F, Zhou L, Dang S, Sun L, Li X, Wang J, Shi Y. Structure and mechanism of an amino acid antiporter. *Science*. 2009; 324:1565–1568. [PubMed: 19478139]
21. Gao X, Zhou L, Jiao X, Lu F, Yan C, Zeng X, Wang J, Shi Y. Mechanism of substrate recognition and transport by an amino acid antiporter. *Nature*. 2010; 463:828–832. [PubMed: 20090677]
22. Kowalczyk L, Ratera M, Paladino A, Bartoccioni P, Errasti-Murugarren E, Valencia E, Portella G, Bial S, Zorzano A, Fita I, Orozco M, Carpene X, Vzquez-Ibar JL, Palacn M. Molecular basis of substrate-induced permeation by an amino acid antiporter. *Proc Natl Acad Sci USA*. 2011; 108:3935–3940. [PubMed: 21368142]
23. Krishnamurthy H, Piscitelli CL, Gouaux E. Unlocking the molecular secrets of sodium-coupled transporters. *Nature*. 2009; 459:347–355. [PubMed: 19458710]
24. Abramson J, Wright E. Structure and function of Na^+ -symporters with inverted repeats. *Curr Opin Struct Biol*. 2009; 19:425–432. [PubMed: 19631523]
25. Perez C, Koshy C, Ressl S, Nicklisch S, Krmer R, Ziegler C. Substrate specificity and ion coupling in the Na^+ /betaine symporter betp. *EMBO J*. 2011; 30:1221–1229. [PubMed: 21364531]
26. Veenstra M, Lanza S, Hirayama BA, Turk E, Wright EM. Local conformational changes in the *Vibrio* Na^+ /galactose cotransporter. *Biochemistry*. 2004; 43:3620–3627. [PubMed: 15035632]
27. Parent L, Supplisson S, Loo DDF, Wright EM. Electrogenic properties of the cloned Na^+ /glucose cotransporter: I. voltage-clamp studies. *JMB*. 1992; 125:49–62.
28. Parent L, Supplisson S, Loo DDF, Wright EM. Electrogenic properties of the cloned Na^+ /glucose cotransporter: Part II. a transport model under non rapid equilibrium conditions. *JMB*. 1992; 125:63–79.
29. Li J, Tajkhorshid E. Ion-releasing state of a secondary membrane transporter. *Biophys J*. 2009; 97:L29–L31. [PubMed: 19948113]
30. Zomot E, Bahar I. The sodium/galactose symporter crystal structure is a dynamic, not so occluded state. *Mol Biosyst*. 2010; 10:1039/b927492h
31. Boudker O, Verdon G. Structural perspectives on secondary active transporters. *Trends in Pharmacological Sciences*. 2010; 31:418–426. [PubMed: 20655602]
32. Sujatha M, Balaji PV. Identification of common structural features of binding sites in galactose-specific proteins. *Proteins*. 2009; 55:44–65. [PubMed: 14997539]
33. Abramson J, Smirnova I, Kasho V, Verner G, Kaback HR, Iwata S. Structure and mechanism of the lactose permease of *Escherichia coli*. *Science*. 2003; 301:610–615. [PubMed: 12893935]
34. Gordon, JC.; Myers, JB.; Folta, T.; Shoja, V.; Heath, LS.; Onufriev, A. H++: a server for estimating pK_as and adding missing hydrogens to macromolecules; Nucleic Acids Res. 2005. p. W368-371. Retrieved September 29, 2010, from [Http://biophysics.cs.vt.edu/H++](http://biophysics.cs.vt.edu/H++)
35. Humphrey W, Dalke A, Schulten K. VMD – Visual Molecular Dynamics. *J Mol Graphics*. 1996; 14:33–38.

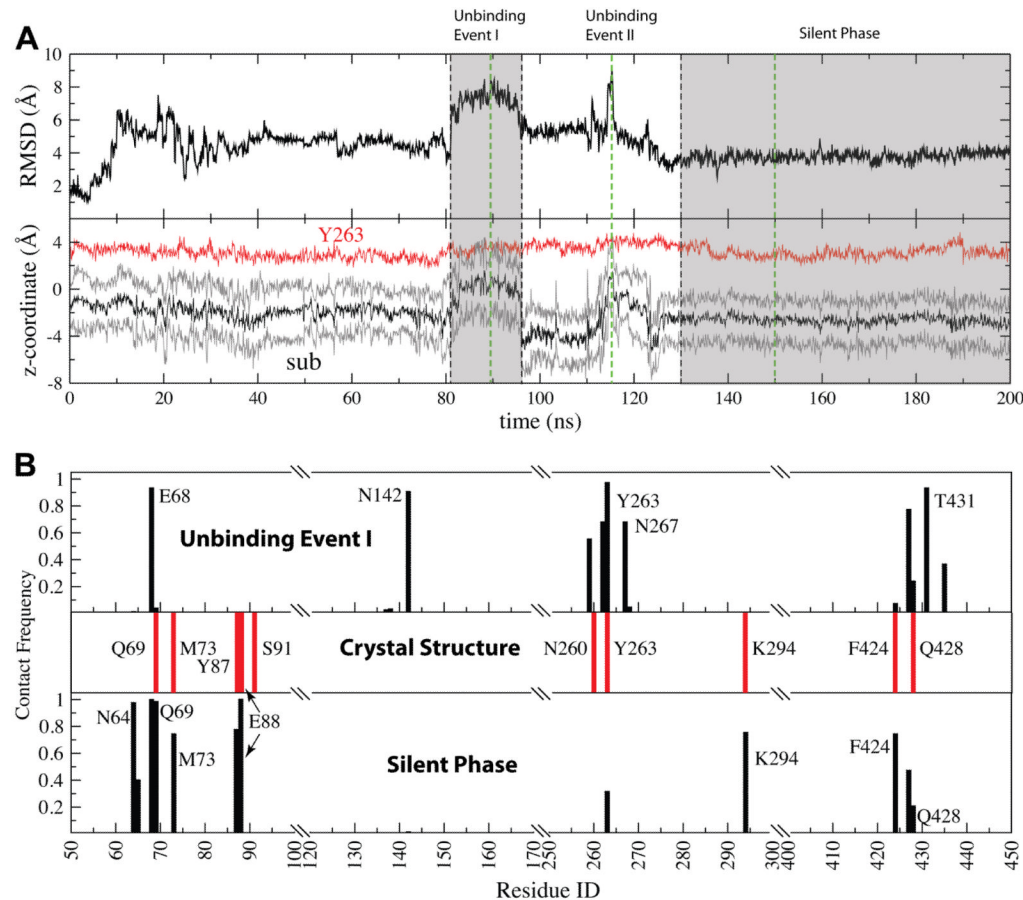
36. MacKerell AD Jr, Bashford D, Bellott M, Dunbrack JRL, Evanseck J, Field MJ, Fischer S, Gao J, Guo H, Ha S, Joseph D, Kuchnir L, Kuczera K, Lau FTK, Mattos C, Michnick S, Ngo T, Nguyen DT, Prodhom B, Roux B, Schlenkrich M, Smith J, Stote R, Straub J, Watanabe M, Wiorkiewicz-Kuczera J, Yin D, Karplus M. Self-consistent parameterization of biomolecules for molecular modeling and condensed phase simulations. *FASEB J.* 1992; 6:A143–A143.
37. MacKerell AD Jr, Bashford D, Bellott M, Dunbrack RL Jr, Evanseck JD, Field MJ, Fischer S, Gao J, Guo H, Ha S, Joseph D, Kuchnir L, Kuczera K, Lau FTK, Mattos C, Michnick S, Ngo T, Nguyen DT, Prodhom B, Reiher IWE, Roux B, Schlenkrich M, Smith J, Stote R, Straub J, Watanabe M, Wiorkiewicz-Kuczera J, Yin D, Karplus M. All-atom empirical potential for molecular modeling and dynamics studies of proteins. *J Phys Chem B.* 1998; 102:3586–3616.
38. MacKerell AD Jr, Feig M, Brooks CL III. Extending the treatment of backbone energetics in protein force fields: Limitations of gas-phase quantum mechanics in reproducing protein conformational distributions in molecular dynamics simulations. *J Comp Chem.* 2004; 25:1400–1415. [PubMed: 15185334]
39. Zhang L, Hermans J. Hydrophilicity of cavities in proteins. *Proteins: Struct, Func, Gen.* 1996; 24:433–438.
40. Lomize, MA.; Lomize, AL.; Pogozheva, LD.; Mosberg, HI. Opm: Orientations of proteins in membranes database; Bioinformatics. 2006. p. 623–625. <http://opm.phar.umich.edu/>
41. Grubmüller, H. Solvate 1.0. 1996.
42. Phillips JC, Braun R, Wang W, Gumbart J, Tajkhorshid E, Villa E, Chipot C, Skeel RD, Kale L, Schulten K. Scalable molecular dynamics with NAMD. *J Comp Chem.* 2005; 26:1781–1802. [PubMed: 16222654]
43. Kuttel M, Brandy JW, Naidoo KJ. Carbohydrate solution simulations: Producing a force field with experimentally consistent primary alcohol rotational frequencies and populations. *J Comp Chem.* 2002; 23:1236–1243. [PubMed: 12210149]
44. Jorgensen WL, Chandrasekhar J, Madura JD, Impey RW, Klein ML. Comparison of simple potential functions for simulating liquid water. *J Chem Phys.* 1983; 79:926–935.
45. Ryckaert JP, Ciccotti G, Berendsen HJC. Numerical integration of the Cartesian equations of motion of a system with constraints: Molecular dynamics of *n*-alkanes. *J Comp Phys.* 1977; 23:327–341.
46. Isralewitz B, Gao M, Schulten K. Steered molecular dynamics and mechanical functions of proteins. *Curr Opin Struct Biol.* 2001; 11:224–230. [PubMed: 11297932]
47. Izrailev S, Stepaniants S, Balsera M, Oono Y, Schulten K. Molecular dynamics study of unbinding of the avidin-biotin complex. *Biophys J.* 1997; 72:1568–1581. [PubMed: 9083662]
48. Martyna GJ, Tobias DJ, Klein ML. Constant pressure molecular dynamics algorithms. *J Chem Phys.* 1994; 101:4177–4189.
49. Feller SE, Zhang Y, Pastor RW, Brooks BR. Constant pressure molecular dynamics simulation: The Langevin piston method. *J Chem Phys.* 1995; 103:4613–4621.
50. Darden T, York D, Pedersen LG. Particle mesh Ewald: An $N \cdot \log(N)$ method for Ewald sums in large systems. *J Chem Phys.* 1993; 98:10089–10092.
51. Turk E, Kerner CJ, Lostao MP, Wright EM. Membrane topology of the human Na⁺/glucose cotransporter SGLT1. *J Biol Chem.* 1996; 271:1925–1934. [PubMed: 8567640]
52. Hirayama BA, Loo DDF, Dez-Sampedro A, Leung DW, Meinild AK, Lai-Bing M, Turk E, Wright EM. Sodium-dependent reorganization of the sugar-binding site of SGLT1. *Biochemistry.* 2007; 46:13391–13406. [PubMed: 17960916]
53. Loo DDF, Hirayama BA, Cha A, Bezanilla F, Wright EM. Perturbation analysis of the voltage-sensitive conformational changes of the na+/glucose cotransporter. *J Gen Physiol.* 2005; 125:13–36. [PubMed: 15596535]
54. Longpr JP, Lapointe JY. Determination of the na(+)/glucose cotransporter (SGLT1) turnover rate using the ion-trap technique. *Biophys J.* 2011; 100:52–59. [PubMed: 21190656]

Highlights

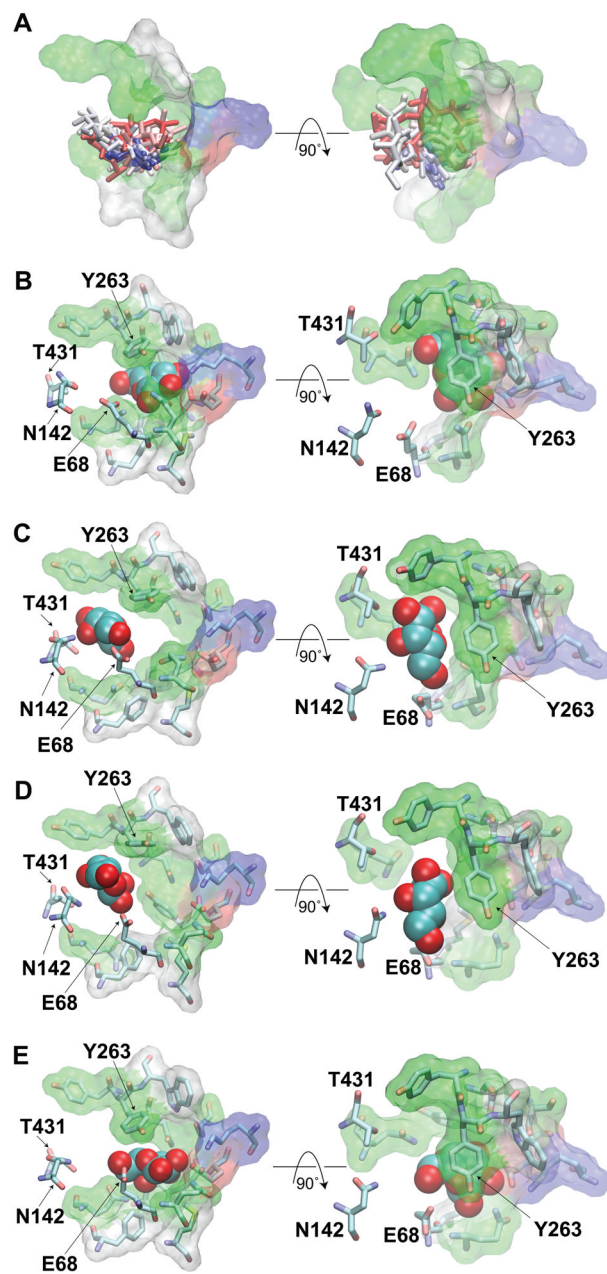
- Equilibrium dynamics of substrate unbinding from the galactose transporter.
- Characterizing the complete release pathway and the role of conserved residues.
- Proposing a gate-free mechanism and pathway for substrate unbinding.
- Proposing that the crystal structure is an open, rather than an occluded state.

**Figure 1.**

Overview of the structure of vSGLT and the simulation system. (A) The simulation system. vSGLT is shown in cartoon representation, with the bound substrate drawn in VDW. The POPE lipids and the ions in solution are also drawn in VDW, while the water is in surface representation. Some lipid molecules have been hidden from the view to provide a clear depiction of the protein. (B and C) The substrate binding site, viewed from within the membrane (B) and from the cytoplasm (C). Important side chains in the substrate binding site along with their individually colored TM helices are explicitly shown and labeled..

**Figure 2.**

Dynamics of the substrate. (A) Substrate's heavy–atom RMSD (top) and its displacement along the membrane normal (z -axis) (bottom) during the 200 ns equilibrium simulation. The position of the substrate along the membrane normal is shown using the maximum and minimum z -coordinate (gray solid lines) and the geometrical center (black solid line) of the substrate, and is compared to the z -position of the geometrical center of the ring of Y263 (red solid line). The gray-colored areas highlight the Unbinding Event I and the Silent Phase. The dashed green lines mark the snapshots that were used as representative ones for the Unbinding Events I and II and for the Silent Phase to initiate the SMD simulations. (B) Substrate contact frequency with residues in vSGLT during Unbinding Event I (top) and the Silent Phase (bottom), compared to that in the crystal structure (middle). A cutoff distance of 3 \AA between any atom from the residue and the substrate is used to define contact with the substrate.

**Figure 3.**

Spontaneous substrate unbinding in the equilibrium simulation. Residues in the substrate binding site are shown in overlaid stick and transparent surface representations. Residues that contact the substrate only during its unbinding from the original pocket, i.e., E68, N142, and T431, are only displayed as sticks. (A) To highlight its significant fluctuation within the binding site, multiple snapshots of the substrate (stick) taken at 10 ns intervals from the 200 ns equilibrium trajectory colored from red to blue according to the time are overlaid. (B–E) Snapshots showing the position and configuration of the substrate (VDW spheres) taken respectively at $t = 0$ ns, 89 ns, 115 ns and 150 ns from the equilibrium simulations.

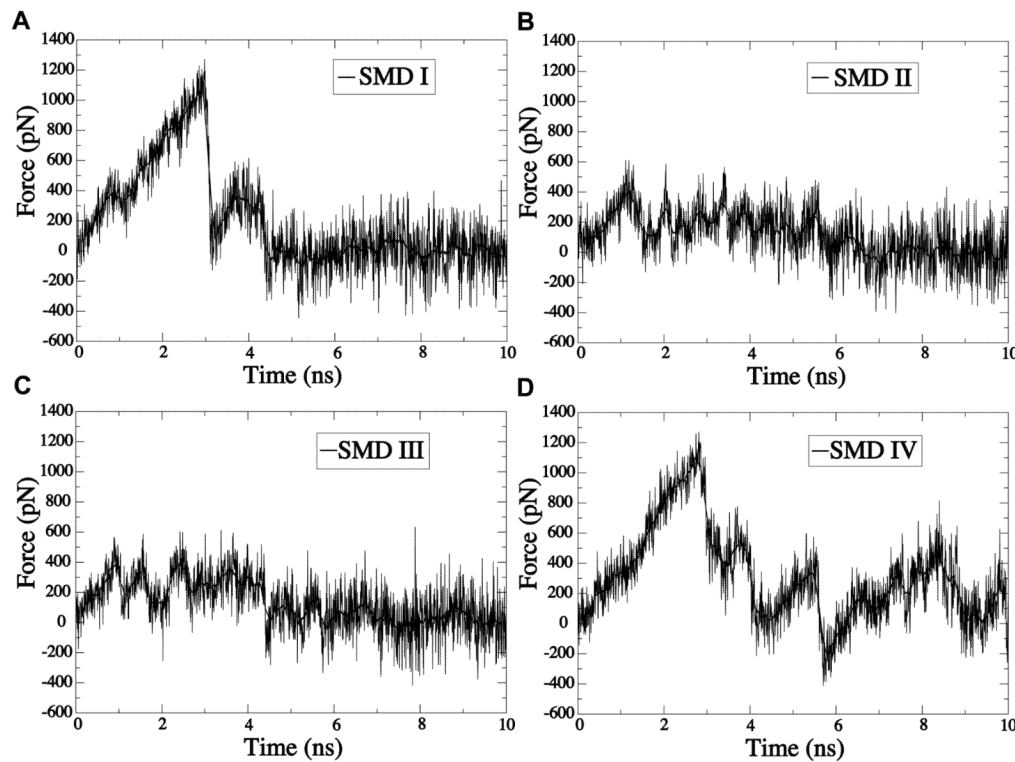
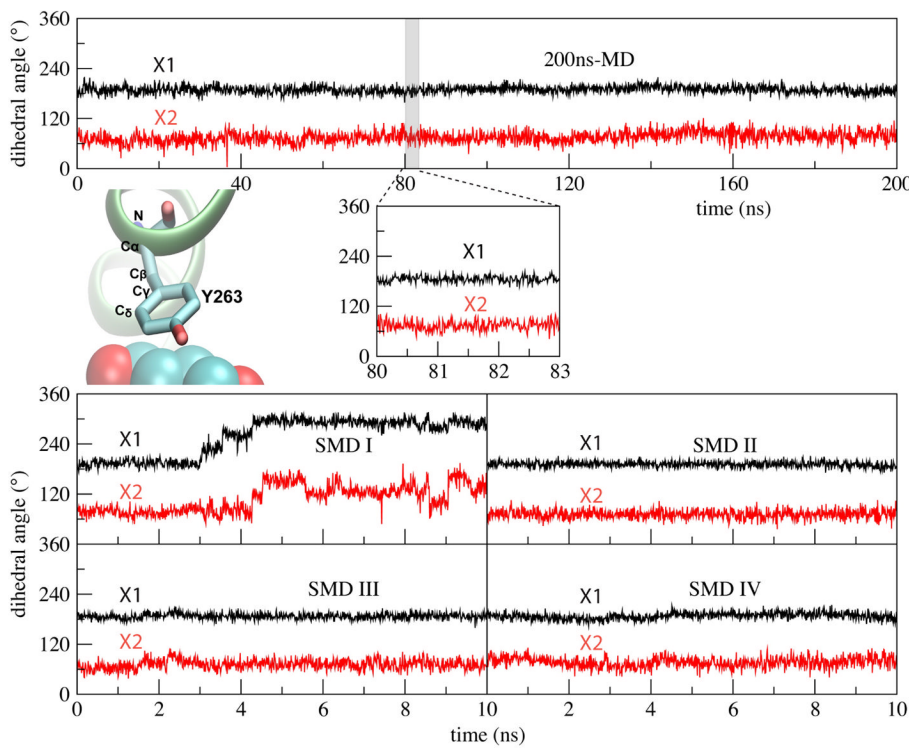


Figure 4.

Force profile in SMD simulations. (A–D) Force-time profiles calculated for induced unbinding of the substrate from vSGLT in SMD simulations I–IV, seeded respectively from snapshots taken from the equilibrium simulation at $t = 0$ ns (crystal structure), $t = 89$ ns (unbound state resulting from Unbinding Event I), $t = 115$ ns (unbound state resulting from Unbinding Event II), and $t = 150$ ns (representative snapshot from the Silent Phase).

**Figure 5.**

Conformational dynamics of Y263 during the simulations. Time series of dihedral angles χ_1 (N-C_α-C_β-C_γ, black lines) and χ_2 (C_α-C_β-C_γ-C_δ, red lines) of Y263 characterizing the conformation of this side chain during the equilibrium and the four SMD simulations. The molecular image shows the relative position of the side chain with respect to the substrate (VDW spheres).

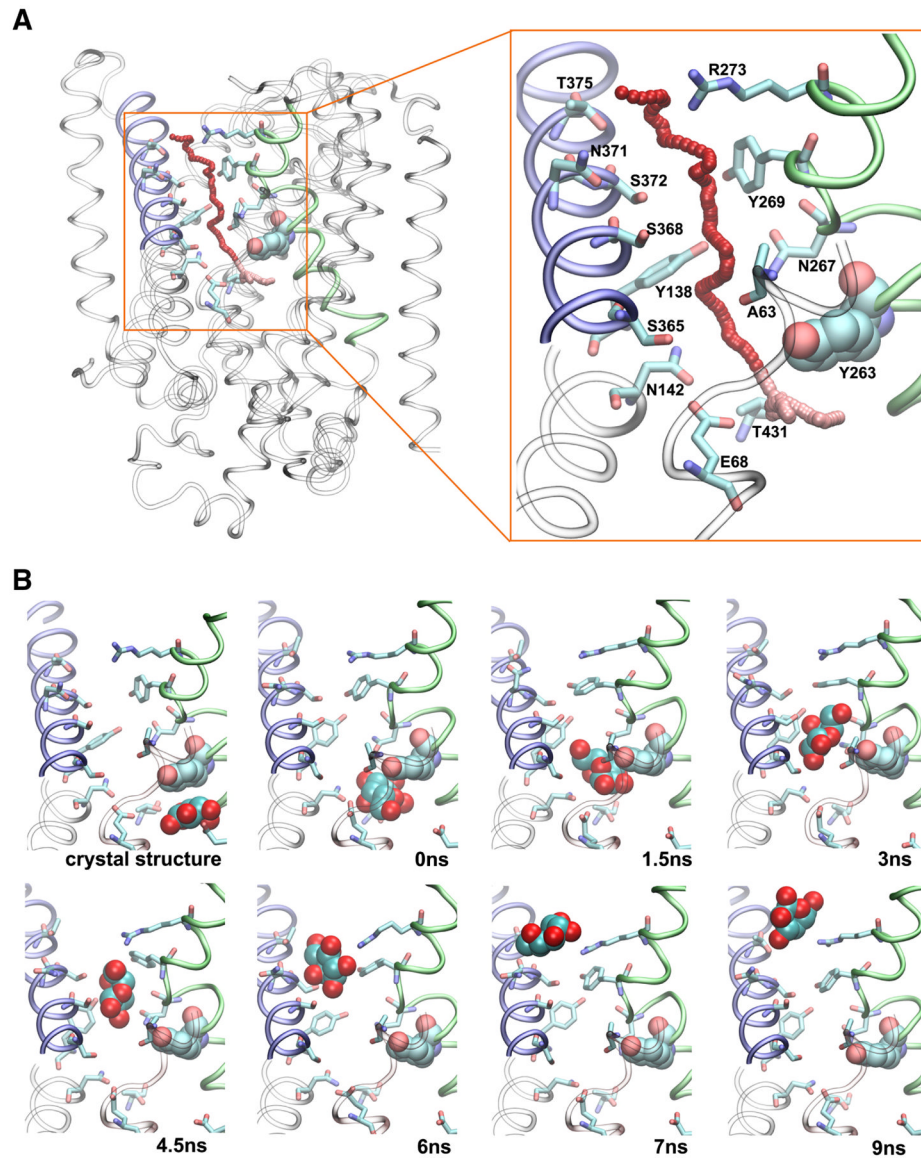


Figure 6.

The cytoplasmic substrate release pathway and mechanism. (A) Overview of the release trajectory of the substrate, obtained by combining the Unbinding Event I taken from the equilibrium trajectory (segment between $t = 80$ ns and $t = 83$ ns of the equilibrium simulation shown using pink spheres) with the unbinding trajectory of SMD-II (red spheres). The spheres specify the position of the C5 atom of the substrate in each frame. The protein is shown in tube representation with the residues lining the substrate's release pathway displayed as sticks and labeled. (B) Snapshots showing the substrate position in the crystal structure ($t = 0$ ns) and at several snapshots along the release pathway taken from the SMD-II simulation.

Table 1

Comparison of the SMD simulations investigating the cytoplasmic substrate release pathway in vSGLT.

SMD	equilibration time (ns)	SMD time (ns)	velocity (Å/ns)	direction <i>a</i>	spring constant <i>b</i>	Y263 blockade ^c	maximum force (pN)
I	0	10	2	z-axis	7	yes	~1300
II	89	10	2	z-axis	7	no	~600
III	115	10	2	z-axis	7	no	~600
IV	150	10	2	z-axis	7	yes	~1300
I ^d	30	10	2	z-axis	7.14	yes	~1200
II ^d	30	10	4	60° to z-axis	7.14	yes	~1100

^aThe z-axis is the membrane normal, with the positive direction being from the extracellular side to the cytoplasmic one as shown in Fig. 1A.

^bkcal/mol/Å².

^cWhether or not the translocation takes place through the space occupied by the side chain of Y263.

^dSMD simulations taken from Zomot's report (30).